Atomic Force Microscope Study of the Effect of the Immobilization Substrate on the Structure and Force−Extension Curves of a Multimeric Protein

Jeffrey G. Forbes,[†,‡] Albert J. Jin,[‡,§] and Kuan Wang*,[‡]

Laboratory of Physical Biology, NIAMS, NIH, Building 6/Room 408, Bethesda, Maryland 20892, and Department of Chemical Engineering, University of Maryland, College Park, Maryland 20742-2111

Atomic force microscopy (AFM) of soluble proteins requires that the protein be immobilized on a flat substrate. Many different substrates have been used successfully for imaging proteins, with mica and gold on mica being the most commonly used. Successful imaging of a soluble protein requires that the protein adhere to the substrate; substrate adhesion is often the primary determinant in choosing a surface for AFM imaging. As a result of the constraint on substrate adhesion, little data is available on how the substrate can affect the conformation of proteins and the resulting images. The AdhE protein of *Escherichia coli* is a multienzyme that forms supramolecular structures composed of 20−60 subunits. We have used atomic force microscopy to study the aggregation state of the purified protein on different substrates and its elastic properties as measured by AFM. We have obtained both contact mode and noncontact (MAC mode) images of the protein assemblies immobilized on a substrate and imaged under buffer. Noncontact mode images on a mica surface show elongated structures as previously observed via electron microscopy, whereas the contact mode images on a gold surface over mica are dominated by globular particles composed of 1−8 monomers. Forced extension of the polypeptide chains yields force versus distance curves which may be fit with the wormlike chain (WLC) model. Our results are consistent with the subnanometer persistence length expected for a typical polypeptide chain. These results indicate that the extension of a protein chain in a supramolecular assembly is not significantly affected by the neighboring proteins.

Introduction

Atomic force microscopy (AFM) has been shown to be highly valuable in the study of many biological samples, from single molecules to cells.[1−5] Two basic functions of the AFM are ultrastructural imaging and force−distance measurements with subnanometer spatial resolution and 10 pN force resolution, respectively. Various modes of AFM operation have been advanced in recent years to suit diverse applications. Proteins are best studied under buffer as their structure may be distorted by the drying and the biological relevance of dry samples may be questioned. However, while under buffer, single proteins are often not immobilized sufficiently well to image with contact mode AFM, because they may be swept away by the scanning of the AFM tip. Some soluble proteins, such as cholera toxin[6] and the chaparonin GroEL,[7−9] will adsorb onto mica in dense monolayers. Although these arrays of

adsorbed protein are not ordered, the close packing allows high-resolution images to be obtained. The imaging of soluble proteins under native conditions, for example, in an aqueous environment, has not yielded as much information as has been obtained for other systems, such as membrane proteins. The two-dimensional order of crystalline arrays of membrane proteins and their ready adhesion to mica surfaces have allowed for detailed imaging of these protein structures.[10−12] Noncontact mode (AC mode) AFM has been shown to be generally more useful for imaging individual proteins under buffer.[5,13−19] In this method of AFM imaging, the cantilever is oscillated and a change in the amplitude of the oscillation is monitored while scanning. The feedback circuitry maintains the position of the tip over the surface by monitoring the drop in the amplitude of the oscillating cantilever when it approaches the surface. In contact mode AFM, the position is maintained by monitoring the applied force which is directly proportional to the cantilever bending. In either mode, the AFM tip is rastered over the sample

* Corresponding author. E-mail: wangk@exchange.nih.gov. Tel: (301) 496-4097. Fax: (301) 402-0009.

† Department of Chemical Engineering, University of Maryland.

‡ Laboratory of Physical Biology, NIAMS, NIH.

§ Current address: Division of Bioengineering & Physical Science, ORS/OD, NIH, Building 13/Room 3N18, Bethesda, MD 20892.

(1) Kasas, S.; Thomson, N. H.; Smith, B. L.; Hansma, P. K.; Miklossy, J.; Hansma, H. G. *Int. J. Imag. Sys. Technol.* **1997**, *8*, 151−161.

(2) Shao, Z. F.; Mou, J.; Czajkowsky, D. M.; Yang, J.; Yuan, J. Y. *Adv. Phys.* **1996**, *45*, 1−86.

(3) Engel, A.; Muller, D. J. *Nat. Struct. Biol.* **2000**, *7*, 715−718.

(4) Nagao, E.; Kaneko, O.; Dvorak, J. A. *J. Struct. Biol.* **2000**, *130*, 34−44.

(5) Thomson, N. H.; Smith, B. L.; Almqvist, N.; Schmitt, L.; Kashlev, M.; Kool, E. T.; Hansma, P. K. *Biophys. J.* **1999**, *76*, 1024−1033.

(6) Mou, J.; Yang, J.; Shao, Z. *J. Mol. Biol.* **1995**, *248*, 507−512.

(7) Mou, J.; Sheng, S.; Ho, R.; Shao, Z. *Biophys. J.* **1996**, *71*, 2213−2221.

(8) Mou, J.; Czajkowsky, D. M.; Sheng, S. J.; Ho, R.; Shao, Z. *FEBS Lett.* **1996**, *381*, 161−164.

(9) Viani, M. B.; Pietrasanta, L. I.; Thompson, J. B.; Chand, A.; Gebeshuber, I. C.; Kindt, J. H.; Richter, M.; Hansma, H. G.; Hansma, P. K. *Nat. Struct. Biol.* **2000**, *7*, 644−647.

(10) Muller, D. J.; Amrein, M.; Engel, A. *J. Struct. Biol.* **1997**, *119*, 172−188.

(11) Muller, D. J.; Engel, A.; Carrascosa, J. L.; Velez, M. *EMBO J.* **1997**, *16*, 2547−2553.

(12) Schabert, F. A.; Henn, C.; Engel, A. *Science* **1995**, *268*, 92−94.

(13) Fritz, M.; Radmacher, M.; Cleveland, J. P.; Allersma, M. W.; Stewart, R. J.; Gieselmann, R.; Janmey, P.; Schmidt, C. F.; Hansma, P. K. *Langmuir* **1995**, *11*, 3529−3535.

(14) Radmacher, M.; Fritz, M.; Hansma, H.; Hansma, P. K. *Science* **1994**, *265*, 1577−1579.

(15) Thomson, N. H.; Fritz, M.; Radmacher, M.; Cleveland, J. P.; Schmidt, C. F.; Hansma, P. K. *Biophys. J.* **1996**, *70*, 2421−2431.

(16) Kacher, C. M.; Weiss, I. M.; Stewart, R. J.; Schmidt, C. F.; Hansma, P. K.; Radmacher, M.; Fritz, M. *Eur. Biophys. J.* **2000**, *28*, 611−620.

(17) Forbes, J. G.; Jin, A. J.; Wang, K., Submitted.

(18) Huang, T. H.; Yang, D. S.; Plaskos, N. P.; Go, S.; Yip, C. M.; Fraser, P. E.; Chakrabartty, A. *J. Mol. Biol.* **2000**, *297*, 73−87.

(19) Lin, H.; Clegg, D. O.; Lal, R. *Biochemistry* **1999**, *38*, 9956−9963.

surface to produce a topological map that reveals surface features of the sample.

The advantage of the AC mode imaging is that the force applied to the surface and the biological material immobilized on the surface can be very small.[20] In contact mode, a contact force >100 pN is typically applied. In AC mode, the applied noncontact force is transient and typically much smaller. More importantly, the lateral force applied to a particle on the surface is also small. With little force applied laterally or onto an immobilized biomolecule, ac mode AFM allows images of these samples to be obtained readily. Imaging in the AC mode also allows the phase shift of the cantilever to be detected, which can yield information on the viscoelastic properties of the material that the cantilever is touching. If the tip touches some material which is soft or sticky, the phase of the cantilever oscillations will lag that of the driving oscillator. This phase information can allow for the detection of biomolecules that may be difficult to image in topographic mode. Early methods of implementing AC mode imaging used a piezoelectric element to oscillate the tip mount, resulting in the mechanical excitation of the cantilever.[21] This technique was a major improvement over contact mode imaging. However, this mechanical excitation of the cantilever performed less well in an aqueous environment, because of the induction of convection currents in the fluid and the damping of some of the modes of the cantilever and the piezodriver itself.[22] It was demonstrated recently that imaging performance in liquid was enhanced by oscillating only the cantilever.[23] The method used for driving the cantilever was to coat the cantilever with a magnetic film and then use an oscillating magnetic field to drive the cantilever. A significant advantage of the magnetic AC (MAC) mode of AFM imaging is that the cantilever may be driven over a wider range of frequencies, which allows for greater control of the instrument.

In addition to imaging, the force-measuring capabilities of the AFM can provide new information on a variety of systems, including biological samples. Forces can be measured with the AFM by first calibrating the force constant of the cantilever and then pushing the tip into a surface and then retracting. Adhesion between the tip and surface is easily recognized by the extension of the force versus distance curve below the baseline. Further retraction from the surface usually results in an abrupt return to the baseline, indicating a rupture of the adhesive interaction between the tip and surface. These types of adhesive properties were the first force measurements made with the AFM and have been useful for characterizing the interactions between different types of surfaces and tip modifications. Over the past several years, a new area of biological force measurement has emerged: the forced extension of biopolymers. The first studies were on polysaccharides,[24,25] which were quickly followed by the cytoskeletal protein titin[26–29] and other proteins.[30–34] With the modular proteins, titin, tenascin, and nacre adhesive, the AFM extension curves are dominated by sequential rupturing or unfolding of the different protein domains, which leads to a sawtooth pattern.[29] The modular nature of these large proteins allows the unfolding of the domains to be clearly separated from the rupture of the tip–surface interaction. Only one study of the extension of a nonmodular, soluble protein has been reported, in which they found that the elastic nature of myelin basic protein depended upon the substrate that it was bound to.[31]

The AdhE enzyme of *Escherichia coli* is a trifunctional enzyme that is required for anaerobic growth of the bacteria, and expression increases 10–15-fold under such conditions. The enzyme contains three Fe^{2+}-dependent enzyme functions: acetaldehyde-CoA dehydrogenase, alcohol dehydrogenase, and pyruvate formate lyase (PFL) deactivase.[35] The acetaldehyde-CoA dehydrogenase function of AdhE is the terminal enzyme in the glycolytic pathway of *E. coli*, converting acetyl-CoA to ethanol and CoA. The preceding reaction in the glycolytic pathway is the conversion of pyruvate and CoA to acetyl-CoA by the free radical enzyme pyruvate formate lyase. A secondary function of AdhE is PFL deactivase which is turned on under microaerobic conditions to protect the active form of PFL from lysis by molecular oxygen. Although homologous proteins have been found in a number of anaerobic and facultatively anaerobic organisms, the only known eucaryotic homologue was found in *Entamoeba histolytica* which causes amebic dysentery and amebic liver abscess.[36,37] This discovery has made the AdhE family of enzymes more interesting as a potential target for antiamebic drugs.

Here, we report the first AFM ultrastructural and forced extension study of AdhE as an example of a protein in a supramolecular assembly. It has been reported that AdhE naturally forms elongated structures which may be isolated from cell lysates and have been called spirosomes because of their helical appearance.[38] The purified protein will also form these elongated structures, and the exact conformation of the monomers in the supramolecular structure depends on the presence of the Fe^{2+} and NAD.[35,39] In the absence of these cofactors, helical structures 15 ± 2 nm in diameter and 45–120 nm long with a left-handed helical pitch of 7.5 nm are formed.[35] In the presence of Fe^{2+} and NAD, longer rods are formed with a diameter of 13.5 ± 1 nm and a helical pitch of 12 nm.[35] Our AFM images reveal that the AdhE multiunit complex retains such helical forms on mica but reorganizes into spherical clusters on gold surfaces. We also show that the AdhE polypeptide can be extended with the AFM and it behaves

(20) Lantz, M.; Liu, Y. Z.; Cui, X. D.; Tokumoto, H.; Lindsay, S. M. *Surf. Interface Anal.* **1999**, *27*, 354–360.

(21) Hansma, P. K.; Cleveland, J. P.; Radmacher, M.; Walters, D. A.; Hillner, P. E.; Bezanilla, M.; Fritz, M.; Vie, D.; Hansma, H. G.; Prater, C. B.; Massie, J.; Fukunaga, L.; Gurley, J.; Elings, V. *Appl. Phys. Lett.* **1994**, *64*, 1738–1740.

(22) Schaffer, T. E.; Cleveland, J. P.; Ohnesorge, F.; Walters, D. A.; Hansma, P. K. *J. Appl. Phys.* **1996**, *80*, 3622–3627.

(23) Han, W. H.; Lindsay, S. M.; Jing, T. W. *Appl. Phys. Lett.* **1996**, *69*, 4111–4113.

(24) Li, H. B.; Rief, M.; Oesterhelt, F.; Gaub, H. E. *Adv. Mater.* **1998**, *10*, 316–319.

(25) Rief, M.; Oesterhelt, F.; Heymann, B.; Gaub, H. E. *Science* **1997**, *275*, 1295–1297.

(26) Rief, M.; Gautel, M.; Schemmel, A.; Gaub, H. E. *Biophys. J.* **1998**, *75*, 3008–3014.

(27) Engel, A.; Gaub, H. *J. Struct. Biol.* **1997**, *119*, 83.

(28) Rief, M.; Gautel, M.; Oesterhelt, F.; Fernandez, J. M.; Gaub, H. E. *Science* **1997**, *276*, 1109–1112.

(29) Wang, K.; Forbes, J. G.; Jin, A. J. *Prog. Biophys. Mol. Biol.* **2001**, in press.

(30) Oberhauser, A. F.; Marszalek, P. E.; Erickson, H. P.; Fernandez, J. M. *Nature* **1998**, *393*, 181–185.

(31) Mueller, H.; Butt, H. J.; Bamberg, E. *Biophys. J.* **1999**, *76*, 1072–1079.

(32) Muller, D. J.; Baumeister, W.; Engel, A. *Proc. Natl. Acad. Sci. U.S.A.* **1999**, *96*, 13170–13174.

(33) Oesterhelt, F.; Oesterhelt, D.; Pfeiffer, M.; Engel, A.; Gaub, H. E.; Muller, D. J. *Science* **2000**, *288*, 143–146.

(34) Smith, B. L.; Schaffer, T. E.; Viani, M.; Thompson, J. B.; Frederick, N. A.; Kindt, J.; Belcher, A.; Stucky, G. D.; Morse, D. E.; Hansma, P. K. *Nature* **1999**, *399*, 761–763.

(35) Kessler, D.; Herth, W.; Knappe, J. *J. Biol. Chem.* **1992**, *267*, 18073–18079.

(36) Yong, T. S.; Li, E.; Clark, D.; Stanley, S. L., Jr. *Proc. Natl. Acad. Sci. U.S.A.* **1996**, *93*, 6464–6469.

(37) Yang, W.; Li, E.; Kairong, T.; Stanley, S. L., Jr. *Mol. Biochem. Parasitol.* **1994**, *64*, 253–260.

(38) Matayoshi, S.; Oda, H.; Sarwar, G. *J. Gen. Microbiol.* **1989**, *135*, 525–529.

(39) Bruchhaus, I.; Tannich, E. *Biochem. J.* **1994**, *303*, 743–748.

like a typical wormlike chain (WLC) polymer with a low persistence length on the order of the peptide bond at 0.38 nm. Our effort also adds insight for other biological applications of AFM.

Experimental Section

Protein Purification. *E. coli* Bl21(DE3) cells were grown in 2 L of LB broth overnight at 37 °C with shaking. The cells were collected and resuspended in 40 mL of lysis buffer (20 mM Na phosphate, pH 7.0, 1 mM EDTA, 0.1 mM DTT, 0.5 mM PMSF (buffer A) with 10 μg/mL leupeptin, 1 mg/mL casein, 1 mM DIFP). The cells were lysed by passing through a French press three times. The cell debris was pelleted by spinning in a SS-34 rotor at 19 500 rpm and 4 °C. The supernatant was then dialyzed overnight at 4 °C in 4 L of buffer A. The crude protein was then centrifuged and applied to a Whatman P11 column (5 × 40 cm) equilibrated in the same buffer at 4 °C. The protein was then eluted with a 0−1 M NaCl gradient over 120 min. Fractions containing the protein were identified by SDS-PAGE and then pooled and dialyzed overnight in 1 L of buffer A. The pooled fractions were then applied to a DEAE Sepharose Fast Flow column. The protein was eluted with a 0−1 M NaCl gradient over 90 min at 4 °C. Fractions containing the protein were identified by SDS-PAGE and then pooled and dialyzed overnight in 1 L of buffer (20 mM Na phosphate, pH 7.0, 0.1 mM DTT). AdhE was purified further by gel filtration chromatography on a Superose-6 or S-500 column in the following buffer: 10 mM imidazole, pH 7.0, 100 mM KCl, 1 mM $CaCl_2$, 2 mM $MgCl_2$ (buffer B) at 4 °C. The gel-purified protein samples were used immediately for imaging and force measurements. For longer term storage, the protein was frozen in liquid nitrogen and stored at −70 °C. Immediately before use, AdhE was purified by gel filtration chromatography as above. The protein concentration of AdhE was determined by absorbance at 280 nm with an extinction coefficient of 0.78 cm^2 mg^{-1}.[40] The purity of the final preparation was 95%, based on SDS gel electrophoresis.[41]

Atomic Force Microscopy. All AFM imaging and force measurements were performed on a Molecular Imaging, Inc. (Phoenix, AZ) PicoSPM atomic force microscope equipped for noncontact imaging (MAC mode). The PicoSPM scans the cantilever over a stationary sample. The cantilever is mounted on a glass rod which may be submersed in the imaging buffer. The X, Y, and Z motion of the piezo element was calibrated on a silicon grating (NT-MDT, Moscow, Russia) with 3 μm between the leading step edges and 20 nm high steps. The X and Y motion of the piezo element was also checked on a packed array of 200 ± 6 nm (NIST traceable) polystyrene nanospheres (Duke Scientific, Palo Alto, CA). The distance between the centers of the beads was within 10% of the expected value of 200 nm. All measurements were taken at room temperature.

AFM Imaging. Both contact mode and AC mode AFM imaging were used in our study. We used the MAC mode for our noncontact ac mode imaging. The contact mode imaging was performed with silicon nitride Microlevers from Park Scientific. The tips were cleaned by immersion in 10% RBS-35 detergent (Pierce) for 1 h to remove organic contaminants. The tips were then exposed to oxygen in the presence of high-intensity UV light to remove any remaining contamination. The ozone generated by the UV light oxidizes any remaining organics on the tip surface. This treatment will also fully oxidize a silicon surface. The AdhE was immobilized on a gold film deposited onto mica (Molecular Imaging). The gold film was first imaged under buffer B to ensure that the surface was flat and clean. The buffer was then removed, and 50 μL of fresh buffer B with 5 mM EDTA was placed in the fluid cell. Then, 5 μL of AdhE at 60 μg/mL in buffer B was added to the fluid cell and gently mixed. After 10 min, the buffer was removed by tilting the fluid cell at ~45° to the scan direction and quickly removing the buffer with blotter paper at the edge of the cell. The fluid cell was then refilled with fresh buffer A with 5 mM EDTA for imaging. The force setpoint was adjusted for a contact force of less than 200 pN. Images were acquired at an image size of 512 × 512 pixels.

The MAC mode imaging was performed with silicon nitride Microlevers from Park Scientific with a magnetic coating applied by Molecular Imaging, Inc. and used without further treatment. These cantilevers are 85 μm long and have a square pyramidal tip and a nominal force constant of 0.5 N/m. Images were acquired with the cantilever oscillating with an amplitude of 5 nm, and the feedback circuitry was set to maintain a drop in the amplitude of the oscillating cantilever of 0.5 nm. AdhE was immobilized on freshly cleaved mica. Low force constant cantilevers such as those used for the contact mode imaging and the force measurements are not suitable for MAC mode imaging because the resonance frequency is too low. When a cantilever is placed in a fluid, the resonance frequency decreases and the width of the resonance broadens. The 300 μm long cantilever used for the contact measurements had a resonance frequency of about 6 kHz which reduced to 1 kHz in buffer. The MAC mode controller is not able to lock onto the oscillations at such low frequencies, and stable imaging is obtained with cantilevers having a higher resonance frequency. The cantilever used for the MAC mode images presented here had a resonance frequency of 60 kHz in buffer.

AFM Force Spectroscopy. Force measurements were made with silicon nitride Microlevers from Park Scientific and silicon nitride coated, silicon ultra-sharp cantilevers from NT-MDT (Moscow, Russia). The silicon nitride Microlevers were cleaned as described above. The cantilevers were calibrated by recording their thermal fluctuations both in air and in buffer and calculating the power spectrum.[42] The error in force constant calibration is ±10%. The force constant of the cantilevers used in this study ranged from 0.019 to 0.03 N/m. For force measurement, the contact forces were kept below 4 nN to reduce the risk of damaging the protein or substrate.

Force versus distance curves were obtained by applying a voltage ramp to the piezo element upon which the cantilever was mounted. As the cantilever moves down and up, the deflection of the cantilever is recorded. When the cantilever touches the surface and bends, the signal becomes more positive as a greater force is applied to the surface. As the tip is retracted from the surface, the tip often sticks to the surface which results in a negative signal (Figure 6D). When the restoring force exceeds the interaction force between the tip and the surface, the cantilever snaps back to its equilibrium position. The cantilever deflection signal is converted to force by first measuring the slope of the deflection when the tip is pressed into a hard surface, which gives the variation of the deflection signal per nanometer. To obtain the force for a given deflection, the deflection signal is divided by the slope and then multiplied by the force constant of the cantilever. This interaction force can be read directly from the force versus distance plots as the difference between the equilibrium position and the bottom of the negative peak. The error in the force measurements is limited by the noise in the deflection sensor and is ca. ±10 pN. In the presence of protein, additional negative peaks can be seen with a curved leading edge which is indicative of elastic extension. Force curves showing elastic extension of the immobilized protein were fit to the WLC model,

$$f = \left(\frac{k_B T}{P}\right)\left[\frac{1}{4(1 - z/L)^2} - \frac{1}{4} + \frac{z}{L}\right]$$

where P is the elastic persistence length, $k_B T$ is the thermal energy, and L is the length of the peptide chain being stretched.[43] Generalized nonlinear least-squares fitting of individual force curves against this model produces the descriptive parameters for AdhE elasticity. Numerical procedures for such fittings and statistical treatments of the resulting parameters were performed using custom programs in MathCad (Mathsoft, Cambridge, MA).

AFM Sample Substrates. Mica and gold evaporated onto mica were used as substrates for protein attachment and AFM studies. Mica is a layered aluminosilicate mineral which is easily cleaved to generate atomically flat surfaces. The surface of mica has a net negative charge which can bind divalent cations, which

(40) Gill, S. C.; von Hippel, P. H. *Anal. Biochem.* **1989**, *182*, 319−326.

(41) Laemmli, U. K. *Nature* **1970**, *227*, 680−685.

(42) Hutter, J. L.; Bechhoefer, J. *Rev. Sci. Instrum.* **1993**, *64*, 1868−1873.

(43) Bustamante, C.; Marko, J. F.; Siggia, E. D.; Smith, S. *Science* **1994**, *265*, 1599−1600.
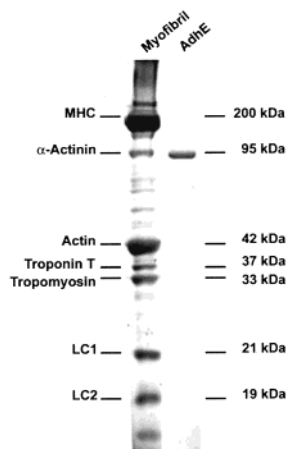
Figure 1. SDS-PAGE of AdhE: lane 1, myofibril molecular weight standard; lane 2, AdhE following size-exclusion chromatography. Lane 2 is representative of the purity of the protein preparations used in this study.

renders the surface positively charged. Many proteins bind tightly to a clean mica surface because of the large surface charge and hydrogen bonding between the protein and the surface. Although tight binding to a substrate can often be beneficial for AFM imaging, the strong surface charge on mica can cause protein aggregation. In some circumstances, the strong interaction between the mica and protein can lead to a distortion of the protein molecule. Gold films can provide a substrate which reduces the charge−charge interactions between the surface and the protein. Proteins interact with gold through the sulfur in cysteine residues and hydrophobic interactions with molecules that rapidly adsorb onto gold. Gold can form atomically flat islands on mica when evaporated onto mica under suitable conditions. These islands can be hundreds of nanometers across, making these gold films ideally suited for AFM imaging and force measurement. Gold films have an additional advantage for AFM imaging in that thiols react readily with the gold, which allows a variety of surface modifications to be made. It is this thiol reactivity which allows proteins to bind to gold through surface cysteine residues. Proteins will also interact with a gold surface through physisorption; however, the interaction is not as strong as that between proteins and mica.

Results

AdhE was isolated from *E. coli* cells grown under aerobic conditions, because it was previously demonstrated that the protein is expressed under aerobic conditions in rich media.[38] Our preparation of the protein was greater than 95% pure, as indicated by SDS-PAGE, Figure 1, and its identity was confirmed by mass spectrometry at 95 995 Da and by partial protein sequencing (Sinz, A.; Ma, K.; Wang, K. Unpublished data).

Figure 2A shows a contact mode image of gold on mica imaged under buffer. The image is 1.7 μm on a side, and the height range has been adjusted to be comparable to the gold surface with bound protein shown in Figure 2B. The image in Figure 2A clearly shows the gold islands that form on mica. One of the islands is over 700 nm across. Although the islands can exhibit a surface roughness of several angstroms, the overall surface is much rougher with some of the crevasses being several nanometers deep. Figure 2B shows a gold film after AdhE has been deposited as described above. The protein assemblies are clearly visible, and there is no doubt that the surface has been modified by the protein. This image was taken in contact mode with a soft cantilever having a force constant of 0.023 N/m. Because a crystal structure is not available for AdhE, which, if any, of its nine cysteines may be binding to the gold cannot be determined.

Figure 3 shows contact mode AFM images of a 500 × 500 nm field of AdhE immobilized on gold. Figure 3A is a topographic mode image of the protein complexes, which clearly shows that the supramolecular assemblies are heterogeneous in size. Analysis of the image indicates that there are three height ranges of the particles and they are roughly spherical. The three classes of structures have average heights of 3.6 ± 0.5, 5.8 ± 0.8, and 8.4 ± 0.4 nm. In these contact mode images, the height of the particles is the actual height of the protein under compression by the tip. However, the width of the particle is a convolution of the actual shape of the particle and the shape of the tip. A spherical particle with a mass of 96 kDa and a density of 1.35 gives an estimated diameter of 6.1 nm. The smaller particles with an average height of 3.6 nm are most likely monomers of AdhE which have been compressed by the loading of the tip. The Park Scientific Microlever used for obtaining this image has a pyramidal tip with a 70° cone angle and a spherical apex with a radius of curvature of less than 50 nm. The expected width at the base of the image of a spherical particle imaged with a spherical tip can be estimated by the simple relationship $W \cong 4\sqrt{R_t}\sqrt{R_p}$, where R_t is the radius of curvature of the tip, R_p is the radius of curvature of the particle being imaged, and $R_t > R_p$.[44] The three particles shown in cross section in Figure 3A have heights of 7.85, 8.0, and 12.9 nm and widths of 51.8, 44.9, and 77.1 nm. Using a radius of curvature for the tip of 30 nm, expected widths of 43.4, 43.8, and 55.6 nm are obtained. By this simple analysis, the protein complexes appear to be nominally spherical; however, the larger ones appear to be wider than expected. The particle with a height of 12.9 nm is the tallest feature in the image and does not lie in any of the three height categories defined by the other features in the image.

Figure 3B is the error signal image corresponding to the topographic image in Figure 3A. The error signal is the difference between the force setpoint and the actual deflection of the cantilever. The error signal image can show fine details, which may be masked by the large dynamic range represented by the color scale of the topographic image. The error signal image clearly shows that the larger protein aggregates are not smooth spheres as might be inferred from the topographic image Figure 3A. The error mode image also indicates that the smaller particles (AdhE monomers) have depressions in them, some of which can be seen in the topographic mode image. These depressions are most likely portions of the protein which are more susceptible to compression from the tip. These features are not seen in the larger aggregates because the protein molecules help support the neighboring molecules which would make the complex more rigid.

Figure 4 shows two MAC mode images of AdhE immobilized on mica and imaged under buffer B. The image in Figure 4B was taken immediately after the image in Figure 4A. These images show some of the same types of particles as seen with contact mode AFM, Figure 3B. An additional feature seen in these MAC mode images is the occurrence of elongated structures similar to those seen in negative stained electron microscopy images. An interesting feature of the image is that most of the particles are of similar height. The taller features are clearly larger aggregates and are probably multiple layers. Measurement of the height of a population of the smaller features yields an average height of 3.7 ± 0.4 nm. This height is

(44) Vesenka, J.; Guthold, M.; Tang, C. L.; Keller, D.; Delaine, E.; Bustamante, C. *Ultramicroscopy* **1992**, *42*, 1243−1249.
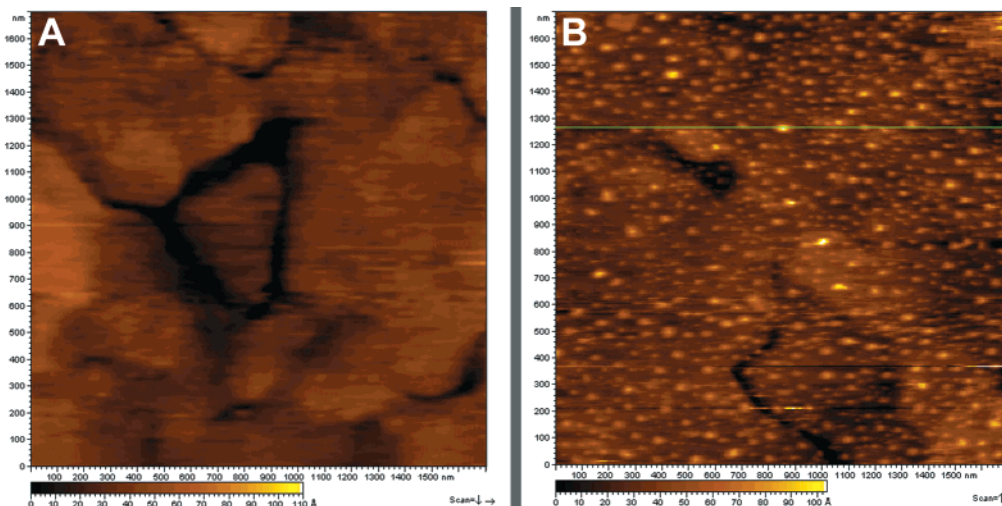
Figure 2. Contact mode images of a gold film on mica without adsorbed protein (A) and with adsorbed protein (B) taken under buffer. Images were taken with a cantilever with a force constant of 0.023 N/m. The images are from different areas of the gold film. The contrast of the image of the bare gold in (A) was adjusted to be similar to that of the gold substrate with the attached protein. The gold islands typically have a height variation of several angstroms, whereas the protein particles vary from 4 to 10 nm in height.
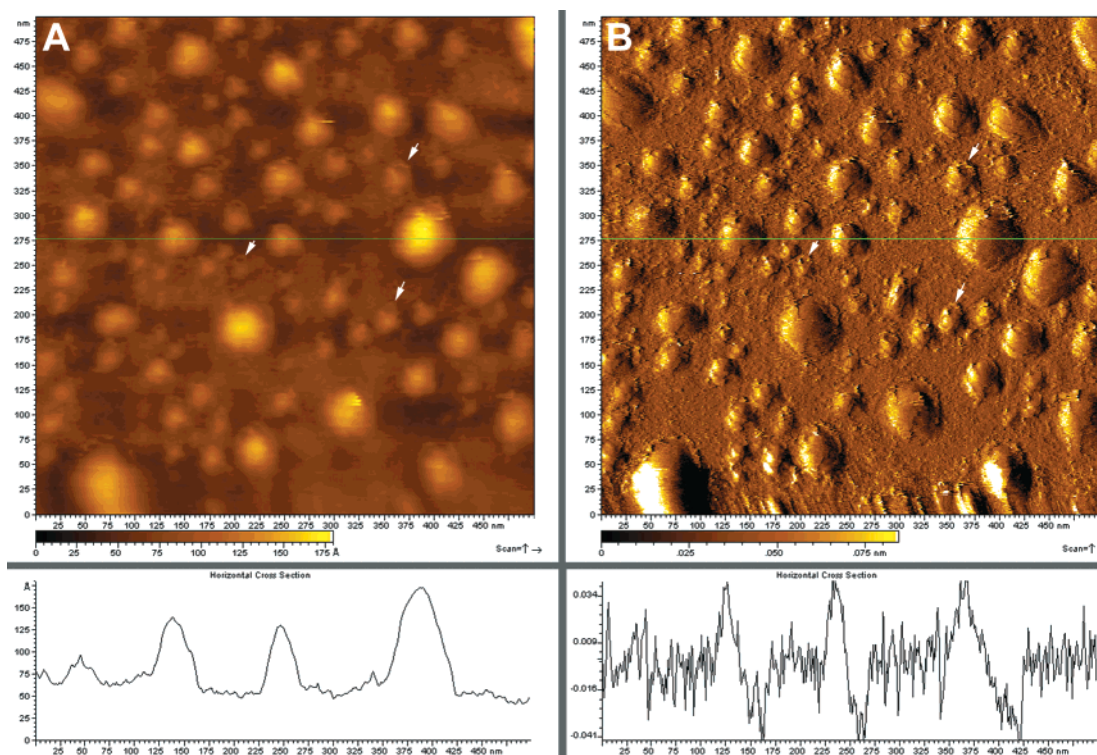

Figure 3. Contact mode AFM images of AdhE immobilized on a gold film taken under buffer B with 5 mM EDTA. This image is an expansion of a portion of Figure 2B: (A) topographic mode image showing the height of the particles on the surface and (B) error signal image. The error signal shows fine details which may be obscured in the topographic image. The arrows in the images point to the protein aggregates which have depressions in them as described in the text. The lower panels are a cross section through the image at the green line. A cantilever with a force constant of 0.023 N/m was used for obtaining these images.

the same as that obtained for the smaller particle in the contact mode image in Figure 3A. A few of the particles in Figure 4A appear to be dimers or higher multimers. The average distance between the centers of mass of the subunits of these multimers is 11.4 ± 0.7 nm. The second scan shown in Figure 4B appears very similar to the preceding scan. With the low lateral force applied by the oscillating cantilever, repeated scans of the surface and attached protein may be expected to be similar. However, some of the particles have moved and others have changed shape. These differences are accentuated in Figure 5. Figure 5A is the same image as Figure 4A except it is

colored red. Figure 5C is the same image as Figure 4B except in green. Image B in Figure 5 is a superposition of images A and C in Figure 5. Where there has been little or no change in the two images, the color is a golden tone similar to the color of Figure 4. A change in position is indicated by the presence of either red or green. There has been a slight drift upward in the second scan as shown by the increase in green at the upper edge of the spherical particle at 75 nm X and 175 nm Y (single arrow in Figure 5B). The particle at 75 nm X and 425 nm Y (double arrows in Figure 5B) has moved much more and taken on a more extended configuration. This is due to the perturbation of
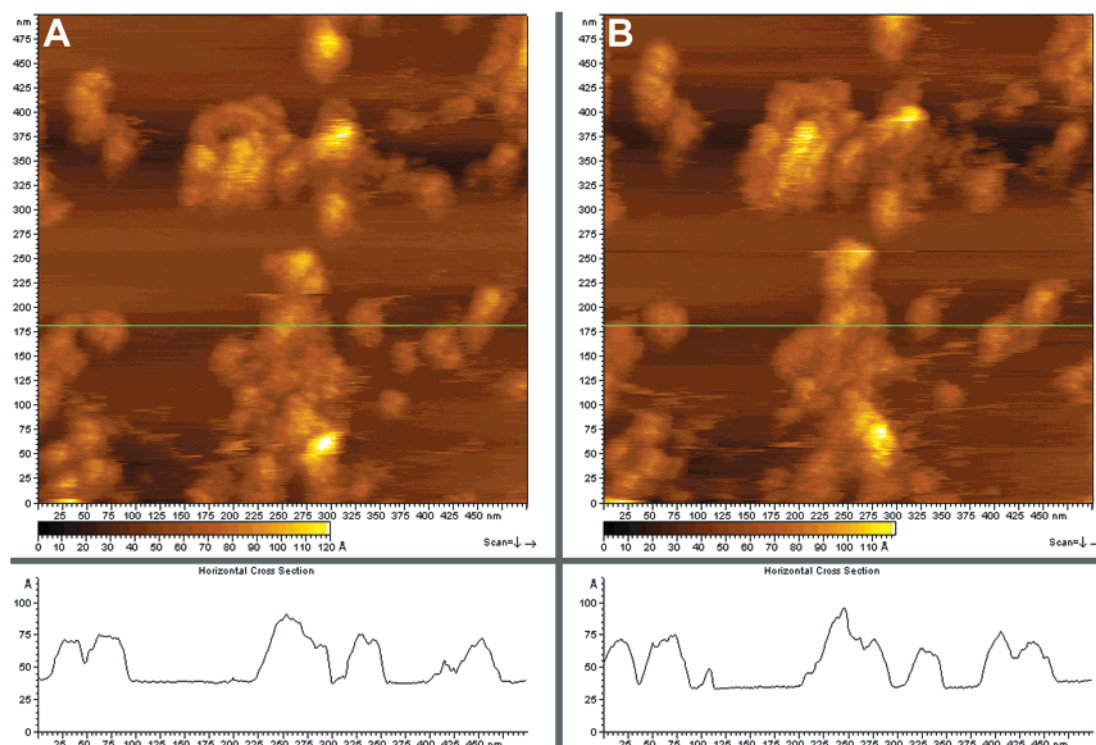
Figure 4. Two MAC mode AFM images of AdhE immobilized on mica. These images were taken under buffer B. (A) A MAC mode image showing the structure of AdhE supramolecular structures. (B) A MAC mode image taken immediately after the image in (A). Comparison of these images shows that the proteins were moved by the AFM tip even in MAC mode, where lateral forces are small. A cantilever with a nominal force constant of 0.5 N/m and a magnetic coating was used for obtaining these images.
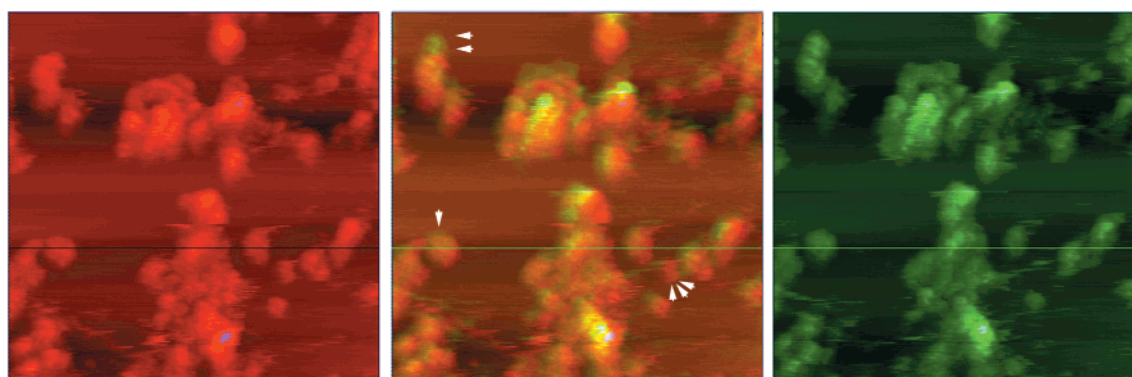

Figure 5. Superposition of MAC mode images in Figure 4 to accentuate the differences of the two scans. (A) The MAC mode image of AdhE shown in Figure 4A colored red. (B) Superposition of the two different MAC mode images of AdhE shown in (A) and (C). The different colors clearly show where the protein particles have moved between the two images. Red regions are more like those in (A), the first scan. Green regions are more like those in (C), the second scan. (C) The mac mode image of AdhE shown in Figure 4B colored green. Arrows point to regions discussed in the text.

the particle by the oscillating tip. Either residual lateral forces moved the particle or transient applied force caused a shape change. Some features have disappeared altogether in the second scan. For example, the particle at 375 nm X and 150 nm Y in Figure 4A is missing from the second scan, as exemplified by the red spot in Figure 5B at the same position (three arrows in Figure 5B).

Figure 6 shows typical force versus distance curves for AdhE immobilized on a gold surface and stretched with a clean silicon nitride tip. Each force versus distance curve is composed of an extension trace and a retraction trace. For the tip−surface interaction in this system, the extension curves show little or no attractive forces between the tip and surface. Upon retraction, an adhesion force is typically observed. The rupture of this adhesive force is indicated by the negative peak on the left side of Figure 6A,B,D.

This adhesive force in the presence of protein is usually less than that for a clean gold surface, and occasionally there is no tip−surface rupture observed, as shown in Figure 6C. As the tip is retracted further from the surface, a curved trace indicating the elastic extension of the polypeptide may be seen, as indicated by the negative peak on the right side of Figure 6A,B and the single negative peak in Figure 6C.

AdhE is composed of 890 amino acids, which would span 338 nm when fully extended, given a peptide bond length of 0.38 nm. In the forced extension curves shown in Figure 6, only a portion of the protein is being extended. The curved portion of the elastic extension curve, for example, Figure 6C, can be fit to the wormlike chain model,[43] which gives a persistence length and a contour length for the polymer being extended. Unlike some previous force spectroscopy studies of proteins where only adhesion is
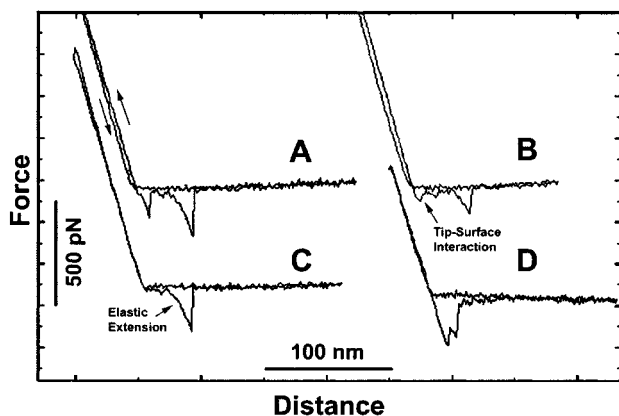
Figure 6. Typical force versus distance curves for AdhE immobilized on a gold film and taken under buffer B. (A and B) Typical force curves that were analyzed in this study. The negative peak on the left of the force curve is the rupture of the tip from the surface. The tip is pressed into the surface which results in a small adhesion between the tip and surface. The larger negative peak is the elastic extension of AdhE. (C) Example of a *F* versus *d* curve where there was no tip–surface rupture, only extension of the protein. (D) Example of a *F* versus *d* curve where there is no elastic extension of the protein. A significant portion of the *F* versus *d* curves were of this type.
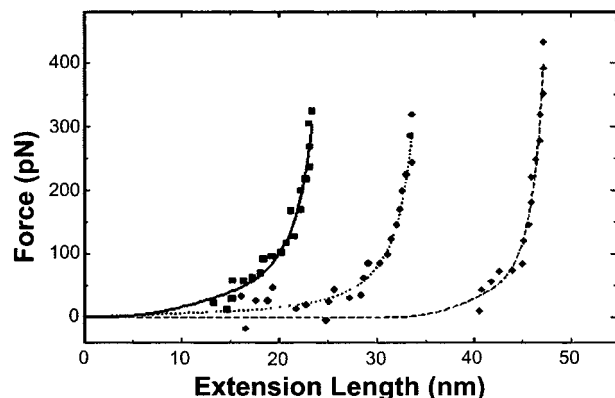
Figure 7. Examples of the elastic extension portion of *F* versus *d* curves as analyzed in this study. The persistence lengths are 0.16, 0.38, and 0.98 nm from left to right.

observed,[45,46] we have observed the elastic extension of the AdhE polypeptide chains with little adhesion. This is indicative of a weak interaction between the protein and the gold surface or a weak interaction between the protein molecules in the supramolecular complex. Figure 7 shows three representative force curves for the extension of AdhE. The point of zero extension is assumed to be where the tip is at its equilibrium position and no longer pressing into the surface. The three force curves in Figure 7 show three different extension contour lengths. Although the interaction between the protein and gold surface may be through a covalent interaction between a cysteine and the gold film, the interaction between the tip and the surface is most likely physisorption, because the rupture forces are well below the force required to rupture covalent bonds.[47] The attachment of the protein to the tip is random, which results in variable lengths of polypeptide being stretched before it ruptures from the tip. The three curves in Figure 7 have contour lengths of 30, 40, and 65 nm and are best fit with persistence lengths of 0.16, 0.38, and 0.98 nm,
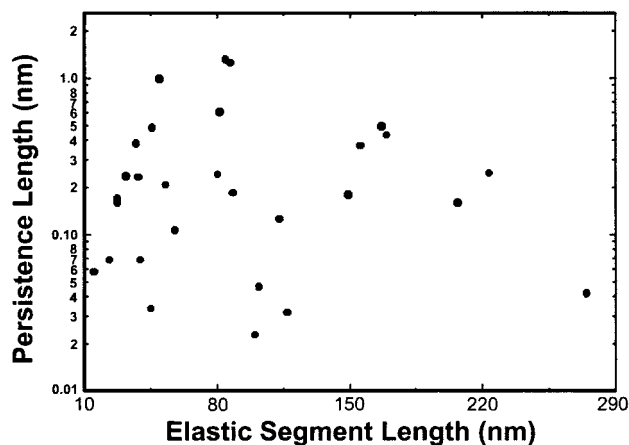
(45) Radmacher, M.; Fritz, M.; Cleveland, J. P.; Walters, D. A.; Hansma, P. K. *Langmuir* **1994**, *10*, 3809−3814.

(46) Sagvolden, G. *Biophys. J.* **1999**, *77*, 526−532.

(47) Grandbois, M.; Beyer, M.; Rief, M.; Clausen-Schaumann, H.; Gaub, H. E. *Science* **1999**, *283*, 1727−1730.

Figure 8. Distribution of persistence lengths versus elastic segment length. The elastic segment length is the length of the polypeptide chain being stretched. The whole AdhE molecule is composed of 890 amino acids which can be stretched a maximum of 338 nm. The actual elastic segment length depends on how the protein is attached to the tip and the gold surface.

respectively. Figure 8 is a plot of the persistence length versus the contour length for the force curves analyzed in this study. Fitting the wormlike chain model to the forced extension data yields both the contour length of the extended protein and the elastic persistence length. As shown in Figure 8, our data yield contour lengths from 15 to 280 nm and elastic persistence lengths from 0.02 to 1.2 nm. The median persistence value is 0.2 nm, and the median elastic contour length is 84 nm. The majority of the persistence length values are between 0.06 and 0.53 nm.

Discussion

AFM images of immobilized AdhE show that the protein retains its supramolecular structures when bound to different substrates. Purified AdhE protein forms elongated multiunit complexes, and the exact conformation of the monomers in the supramolecular structure depends on the presence of the Fe^{2+} and NAD.[35,39] In the presence of these cofactors, the helical pitch of the structure is longer and the protomers are packed less closely making a more open helix with a left-handed pitch of 12 nm, whereas the absence of these cofactors results in a condensed structure with a helical pitch of 7.5 nm. The results reported here are on the condensed structures in the absence of any cofactors.

Figures 3 and 4 show large differences between the images obtained by contact and noncontact force microscopy. Aside from the presence of divalent cations in the buffer used in obtaining the image in Figure 4, they are indeed images of the same protein. Therefore, the different ultrastructure is mostly likely due to distinct protein–substrate interactions. EDTA is used in the protein purification protocol, so any iron bound to the protein, which has been shown to affect the supramolecular structure, is no longer present. The average height of the smaller particles obtained by contact AFM in Figure 3A is 3.6 nm. The average height of the particles obtained by MAC mode AFM is 3.7 nm. As discussed above, the maximum amount of force applied to the protein during imaging by both techniques is approximately the same given the cantilevers and setpoints used for obtaining the images. Given that the heights of the particles obtained by the two different imaging modes are nearly identical, we have imaged monomers and multimers of AdhE by the two different techniques. The differences in the overall shape of the particles shown in Figures 3 and 4 can be accounted for

if the orientation of the structures in relationship to the substrate are different for immobilization on gold and mica. A similar effect in substrate binding has been seen in Alzheimer's β-amyloid peptide, where the peptide binds randomly to mica but binds along crystallographic axes on highly ordered pyrolytic graphite.[48] Given that AdhE binds tightly enough to gold to withstand the lateral forces applied by the AFM tip, the protein is most likely binding to the gold through surface cysteines. Because there is no crystal structure available for this protein, we can only speculate that at least one of the nine cysteines may be on the surface of the protein. The shape of the particles in the contact mode image of AdhE can be readily explained if the cysteine causes the supramolecular structures to stand on end. If only monomers and the terminal protomer of the supramolecular assembly bind to the gold, then they would stand on end if other interactions between the protein and gold were weak. If the assemblies did indeed bind to the gold at one end, then they would form a polymer brush on the surface and entropic fluctuations would exclude other assemblies from binding too near. This is supported by the homogeneous distribution of the particles over a very large surface area as shown in Figure 2B. These slimly supported structures would be ruptured by the meniscus forces during sample preparation, leaving only the stubs of previously long assemblies. It is also conceivable that the multimers were broken by the scanning of the AFM tip during imaging. This is less likely, because we did not observe any streaking and distortion of the images resulting from contaminated tips. The three classes of particles seen in Figure 3 would then be monomers and structures nominally two and three protomers tall, the variation in the width of the particles being due largely to the convolution of the tip shape with the height of the particle.

The binding of AdhE to mica surfaces leads to completely different images. The calculated pI of AdhE is 6.3, and it would bind only weakly to cleaved mica in a buffer at pH 7.0 in the absence of divalent cations. It has been shown that incubating mica in buffer with Mg^{2+} enhances the binding of DNA to the mica. The divalent magnesium replaces some of the monovalent alkaline metals in the mica surface resulting in the surface becoming positively charged. The images shown in Figure 4 were taken in buffer containing Ca^{2+} and Mg^{2+} which would cause the surface to become positively charged. As with DNA, the negatively charged AdhE would bind to the mica surface through electrostatic interactions. Acidic residues comprise 104 of the 890 total amino acids in the amino acid sequence of AdhE. The majority of these will be on the surface which will give the supramolecular assemblies a negative charge along their length. In contrast to the binding of AdhE to gold, these assemblies will bind to mica lying flat, which is supported by the elongated structures seen in Figure 4. The strong interaction between the protein assemblies and the positively charged mica surface allows the particles to come more closely to one another as is seen in the image.

Comparison of the contact and MAC mode AFM images of AdhE also demonstrates one of the fundamental differences between these two modes of imaging. Although the AdhE assemblies are small in comparison to the overall tip height (3 μm), the particles are of similar size to the apex of the tip (30 nm radius of curvature). However, the apex of the tips is not smooth and has one or more asperities, which is the location of much of the interaction between the sample and the tip during contact mode imaging. It is these asperities which allow atomic resolution of hard surfaces with tips that are nominally orders of magnitude larger than the atoms being imaged. The contact mode image in Figure 3A clearly shows fine details which are absent in the mac mode image shown in Figure 4. Although noncontact mode AFM imaging may not be entirely contact free, this mode of imaging relies upon a long-range interaction between the tip and sample. These long-range interactions cause the images to be more sensitive to the shape of the tip and especially to tips which have more than one prominent asperity. These tip effects result in the "softer" appearance of the image and an apparent lack of fine details. However, noncontact AFM allows images to be obtained of structures which would be disrupted by the force of contact mode imaging. The cantilevers used in this study were of the same type except for the magnetic coating on the MAC tips. Noncontact AFM images are enhanced by the use of sharper tips with a smaller cone angle and radius of curvature at the apex.

The electrostatic interaction between AdhE assemblies and mica is sufficiently strong and over an extended portion of the molecule that force spectroscopy shows only tip–surface rupture and no elastic extension of the molecules. Under these conditions, AdhE (and other proteins) acts like an adhesive between the tip and the mica surface because of multiple interactions between the protein and both surfaces. As shown in Figure 6A–C, elastic extension of the protein is seen when it is bound to gold. Again, the interaction between gold and most of the protein must be weak, whereas the interaction between the AFM tip and the protein is strong. The force at which the polypeptide ruptures from the tip is less than 500 pN which is indicative of physisorption of the protein to the tip, because the sulfur–gold bond is on the order of 1 nN and other covalent bonds are stronger. Fitting the WLC model to the extension data gives both the contour length and the elastic persistence length. As is shown by the graph in Figure 8, there is little correlation between the persistence length and the contour length for stretching AdhE. If the persistence length was identical for each portion of the protein being stretched, then the data points would lie along a horizontal line closely centered around that persistence length. However, if the length of the segment being stretched affected the response of the polymer, then clustering or a linear change in the persistence length with the contour length may be exhibited. The scatter in this plot suggests that some other effects must be coming into play.

Given the large range of our fitted persistence lengths for the extension of AdhE and the small range determined for other proteins, it is apropos to summarize the persistence lengths found for other polymer systems where the WLC model is applicable. The forced extension of titin modules was found to be best fit with a persistence length of 0.39 ± 0.07 nm ($n = 10$),[49] and the peptide bond length is 0.38 nm. The extension of myelin basic protein on mica was fit with a persistence length of 0.5 ± 0.25 nm.[31] The extension of poly(methacrylic acid) was fit with a persistence length of 0.28 ± 0.05 nm.[50] The extensions of polystyrene and poly-2-vinylpyridine chains from films of the polymers were fit with the WLC model and gave elastic persistence lengths ranging from 0.05 to 10 nm.[51] The dispersion in the persistence length found in these studies varied from 20% to over 500%. This large difference in the

(48) Kowalewski, T.; Holtzman, D. M. *Proc. Natl. Acad. Sci. U.S.A.* **1999**, *96*, 3688–3693.

(49) Carrion-Vazquez, M.; Oberhauser, A. F.; Fowler, S. B.; Marszalek, P. E.; Broedel, S. E.; Clarke, J.; Fernandez, J. M. *Proc. Natl. Acad. Sci. U.S.A.* **1999**, *96*, 3694–3699.

(50) Ortiz, C.; Hadziioannou, G. *Macromolecules* **1999**, *32*, 780–787.

(51) Bemis, J. E.; Akhremitchev, B. B.; Walker, G. C. *Langmuir* **1999**, *15*, 2799–2805.

quality of fits of different studies can be attributed to a number of factors. Noise in the data and uncertainty in the starting point of the extensions will induce uncertainty in the fits, although a spread of 500% cannot be easily attributed to these factors. If the data are very noisy, then the data set can be rejected, as the goodness-of-fit predictor (χ^2) will be too large. The uncertainty in the starting point of the extension of the polymer is most likely of similar magnitude in all of the studies. Another factor which must be considered is that the wormlike chain model is an empirical model based upon a polymer composed of identical, noninteracting monomers. Although synthetic polymers and, to a lesser extent, DNA fit these criteria, proteins are heteropolymers with side chains that can interact with one another. Steric interactions can limit free rotation around bonds, and charge−charge interactions can result in enthalpic contributions to the elasticity. As there is no structural basis for the WLC model, polypeptides with similar lengths but different sequences can have different persistence lengths. Furthermore, the persistence lengths determined by fitting the WLC model to single-molecule extension data cannot be compared directly to persistence lengths determined by other means in the absence of tension.[52]

How might these different conditions affect the four studies listed above? The study by Ortiz and Hadziioannou is the most well characterized system studied by single-molecule force spectroscopy so far.[50] The poly(methacrylic acid) used in the study was modified with a single thiol group at one end, and the polymer was deposited onto a gold film in the presence of 11-mercaptododecanol. The short-chain thiol forms a self-assembled monolayer, and the polymer molecules are spaced 100−200 nm apart. The mercaptododecanol monolayer reduces the interaction of the polymer with the surface, and the polymers are unable to interact with one another. This sample preparation gave a dispersion in their fitted persistence length of less than 20%. The study of immunoglobulin domains by Carrion-Vazquez and colleagues also reported a dispersion of persistence lengths less than 20%.[49] The recombinant protein used in this study had two cysteines at the carboxy terminus to allow for the covalent binding of the protein to the gold film. However, the protein was applied at such a concentration as to form a film 20−50 nm thick.[53] Clearly, the proteins may interact with one another in such a thick film if they have a propensity to do so. The dispersion in the persistence length for stretching myelin basic protein was intermediate at 50% with the protein immobilized onto mica.[31] Unlike many other proteins, myelin basic protein must not interact strongly with clean mica. This may be due to the net positive charge on the protein. Finally, the study by Bemis and colleagues reported a large dispersion in their fits of persistence lengths for the stretching of polymers from spin-cast films.[51] Because these films are many molecules thick, the polymers can interact with one another. The results presented here are from supramolecular assemblies of AdhE, so the polymer chains are clearly interacting with one another. Protein−protein interactions are usually between interfaces. These interfaces are often composed of amino acids that are not close to one another in the primary sequence but are neighbors in the folded protein. As a protein is unfolded and stretched, these interfaces are ruptured and how the two proteins interact becomes more difficult to describe. If the polypeptide that is being stretched retains some interaction with its neighbors, then the WLC model will not yield the expected results. As described above, many of the AdhE particles bound to the gold appear to be monomers; as such, they will not be perturbed by the effects of neighbors. Although the interaction between the protein and the gold surface is much weaker than that between mica and AdhE, there may still be physisorption effects which can perturb the extension of the molecule.

The WLC model is appropriate for a single chain which is not interacting with other chains or its surroundings. When the chain is interacting with the substrate, it can behave as if it is stiffer, which would give a larger persistence length. If multiple chains are interacting, then the forces are distributed throughout them and the WLC model will give a shorter persistence length. Furthermore, if bonds in the polymer chain can be stretched, then the elastic behavior of the chain will also deviate from that described by the WLC model. Stretching of bonds in the polypeptide leads to an increase in the length of the molecule. This enthalpic change in the molecular elasticity can be accounted for by adding an additional force term to the WLC model.[54] The presence of an enthalpic component in the molecular elasticity will result in the standard WLC model giving a smaller persistence length than will be found when the enthalpic term is included. The dispersion in our set of persistence lengths for AdhE may be due, in part, to the fact that we are stretching different portions of the protein with different sequences and therefore different persistence lengths and possibly different enthalpic components.

Conclusions

We have demonstrated that the choice of immobilization substrate can have a profound effect upon both the imaging and forced extension of multimeric proteins. The multimeric protein studied here, AdhE, binds well enough to gold to be imaged with contact mode AFM, and yet elastic response curves are also readily obtained from the protein. When AdhE is immobilized on mica, very different images are obtained because of the difference in how the protein interacts with the surface. Although mica is ideal as an imaging substrate, in the case of the protein studied here, it is not useful for forced extension. The data presented here clearly demonstrate that noncontact mode AFM is not always the best or only way of obtaining high-quality images of soluble proteins. Noncontact or AC mode AFM is just one tool for the force microscopist to apply to the system under study. Additionally, the choice of substrate can provide insights into how multimeric proteins interact with their neighbors and their surroundings. The ideal situation in force spectroscopy of polymers is when the polymer being studied is attached to a single point on the surface and a single point on the tip. Additionally, the polymer should not interact with the surface or its neighbors. Of course, ideality rarely occurs, and the interesting systems to be studied by force spectroscopy will be plagued by these problems. Some of these difficulties may be reduced or eliminated by the use of a suitable surface for immobilization and solution conditions.

(52) Rief, M.; Fernandez, J. M.; Gaub, H. E. *Phys. Rev. Lett.* **1998**, *81*, 4764−4767.

(53) Carrion-Vazquez, M.; Marszalek, P. E.; Oberhauser, A. F.; Fernandez, J. M. *Proc. Natl. Acad. Sci. U.S.A.* **1999**, *96*, 11288−11292.

(54) Wang, M. D.; Yin, H.; Landick, R.; Gelles, J.; Block, S. M. *Biophys. J.* **1997**, *72*, 1335−1346.